Experimental Investigation of Flowfield About a Multielement Airfoil

A. Nakayama*
Aerodynamics Research and Technology Group, Douglas Aircraft Company, Long Beach, California
H.-P. Kreplin†
German Association for Research in Air and Space Flight, Göttingen, Federal Republic of Germany
and
H. L. Morgan‡
NASA Langley Research Center, Hampton, Virginia

Detailed measurements of mean flow and turbulence quantities around a multielement airfoil model have been made using pressure and hot-wire probes. The results obtained in two test cases at chord Reynolds number of 3×10^6 and freestream Mach number of 0.2 show a number of features of the complex flows that are important for accurately modeling these flows by numerical methods. Many parts of the shear flow deviated vastly from classical flows, and the interaction with the external potential flow is very strong.

Nomenclature

c = model chord length in stowed position [$c = 22$ in. (55.9 cm) for present model]
C_D = drag coefficient
C_f = skin-friction coefficient [$\equiv (\tau_w/\frac{1}{2}\rho U_e^2$]
C_L = lift coefficient
C_p = static pressure coefficient [$\equiv (p - p_{\text{ref}})/\Delta P_{\text{ref}}$]
G_F = gap between spoiler trailing edge of main element and flap
G_s = gap between slat trailing edge and main element
M = Mach number
O_F = overhang along the main chord line of the flap leading edge to the spoiler trailing edge
O_s = overhang along the main chord line of the slat trailing edge to the main element leading edge
p = inflow static pressure
Re = Reynolds number based on chord length
u = fluctuating velocity component in x direction
U = mean velocity in x direction
U_{ref} = tunnel reference velocity
v = fluctuating velocity component in y direction
V = mean velocity component in y direction
w = fluctuating velocity component in z direction
W = mean velocity component in z direction
x = streamwise coordinate, parallel to local model surface in boundary layers and perpendicular to traverse direction in wake
X = distance along the chord line of the model and its extension in wake
y = cross-stream coordinate perpendicular to x direction
z = spanwise coordinate
α = angle of attack
δ_F = flap deflection angle
δ_s = slat deflection angle
ν = kinematic viscosity of air
ρ = density of air
τ = shear stress

Subscripts

e = quantities at edge of boundary layer
w = values on the model surface
ref = tunnel reference value

Presented as Paper 88-2035 at the AIAA 15th Aerodynamic Testing Conference, San Diego, CA, May 18–20, 1988; received May 24, 1988; revision received Feb. 2, 1989.

*Principal Engineer Scientist. Member AIAA.
†Aerodynamics Branch.
‡Aerospace Engineer.

Introduction

WHILE notable progress is being made in the development of methods of computing flows around single airfoils, including flow separations at subcritical speeds,[1] methods that compute flow around high-lift systems of multielement airfoils, including realistic representations of complex shear flows, do not exist, and development efforts are currently being made. The complex geometric configurations and the resulting complexity of the physics of the flow mechanisms of such systems make the task very difficult if details of the shear flows are to be modeled. At present, due to the scarcity of experimental data that contain sufficient details of the flowfield, it is not even clear what features need to be modeled and to what level of sophistication.

Among the few published data on multielement airfoil flows.[2–4] the low-speed test data of Ref. 3, which appear to be the most extensive and detailed, reveal a number of features that draw the attention of computational modelers. They include small- and large-scale separations, complex interacting shear layers, highly curved boundary layers, and near wakes. In most high-lift cases, the viscous-inviscid interaction appears to be strong.

There are some other published data on the flowfield of wing-flap configurations such as those of Refs. 5 and 6, but these are mostly pitot-tube data of mean velocity distributions on somewhat simplified geometry at relatively low Reynolds numbers. It is clear that experimental data are needed that contain the detailed information including turbulence characteristics of shear flows about realistic multielement airfoils under realistic flying conditions. The experimental work reported here is a detailed investigation of flows, primarily the

shear flows, around a three-element airfoil model at a realistic Mach number and moderately high Reynolds number. The mean flow and turbulence characteristics have been obtained using pressure and hot-wire probes. It is intended to map the flowfields for a few representative test cases so that the results can be used for guiding the development and testing of computational methods.

Experimental Arrangement

Wind Tunnel

Due to its unique capabilities for the study of two-dimensional high-lift systems at high Reynolds numbers, NASA Langley Research Center's Low Turbulence Pressure Tunnel (LTPT) was used for the present work. It is a pressurized, closed-circuit, continuous-flow wind tunnel. Its 7.5-ft (230-cm) -high, 3-ft (91-cm) -wide test section is designed for two-dimensional testing of wing sections and is equipped with a blowing system for sidewall boundary-layer control (BLC). References 7 and 8 give the details of this facility. At the present nominal test condition of 0.2 Mach number and 3×10^6 chord Reynolds number, the velocity fluctuations in the test section as reported in Ref. 8 are about 0.1%.

Multielement Airfoil Model

The multielement airfoil model studied in the present work is a three-element airfoil with a conventional slat and a single-segment flap. The chord length c of the model in the clean airfoil configuration with the slat retracted and the flap stowed is 22 in. (56 cm). The chord lengths of the slat, the main airfoil, and the flap are 14.5, 83, and 30%, respectively, of the clean airfoil chord c. Airfoil elements are held together normally at four spanwise positions at 9.5-in. (24.1-cm) intervals by means of brackets. However, to obtain flow condition with minimal three dimensionality, one of the inboard slat brackets was left out (see Fig. 3) during the flowfield survey done at one-sixth of the highest Reynolds number for which the model is designed. No artificial boundary-layer transition fixing was tried on any surface since "tripping" was not considered to be appropriate on confluent boundary layers on multielement airfoils. More information about the model is given in Ref. 9.

Survey Probes and Traverser

Figure 1 is a side-view sketch of the probe traversing system used in the present measurements. The traverser is designed with enough degrees of freedom so that probes can be positioned in various parts of the flow. The entire structure was mounted on a vertical strut fixed at about two model chord lengths downstream of the model trailing edge. Once the probes are positioned at the known first position, the combination of motions in two directions controlled by the computer can automatically move the probes to the rest of the preprogrammed positions within an error of about 0.1 mm. When the boundary layers were surveyed, the first position was the closest point to the model surface where the probes could safely be placed.

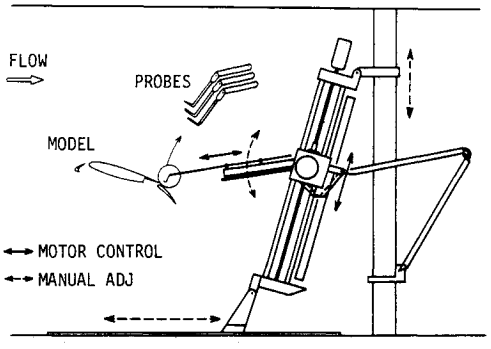

Fig. 1. Sketch of probe traverser.

Turbulence quantities as well as mean velocity components were measured by a special subminiature triple-wire probe shown in Fig. 2. The probe was custom made and had distinctive features compared with commercially available probes. First, the present probe used thin and short sensors (2.5-μm-diam tungsten wire of active length 0.5 mm) so that the overall spatial resolution was much better. The sensing elements were contained inside a sphere with a diameter of 1.2 mm or less. The second special feature of the present probe was that two of the three sensors were arranged in the form of a shifted X or the shape of the Greek letter Λ so that the outputs from these two sensors could be processed like those from the usual X-wire probes. The third sensor was placed between the other two in the plane parallel to the probe axis but perpendicular to the plane formed by the other two sensors. The output was analyzed together with the other two outputs to determine the spanwise velocity component.

To supplement and cross-check the mean velocity results of the triple-wire probe data, a five-hole pressure probe was traversed together with the other probes. The five-hole probe gave the local total and static pressures along with magnitudes and the directions of the mean velocity vectors.

The geometry of the five-hole probe used in the present experiments is described in Ref. 10. This probe has good angle sensitivities over the range of yaw and pitch angles between ± 30 deg relative to the direction of the probe axis.

In addition to these probes, a flattened pitot tube was used in parallel. The stem length and the diameter were made identical to other probes. The tip of the probe was as thin as 0.2 mm so that flow very close to the surface could be measured. Since this type of probe is very sensitive to the flow direction, the primary use of the results was to study the near-surface flow properties.

Data Acquisition and Reduction

All data including the tunnel static and total pressures and temperature were acquired through an analog-to-digital converter or through the IEEE-488 communication line into a graphics computer. This system was operated totally independently of the tunnel data acquisition system, which was used for the purpose of adjusting the tunnel conditions and acquiring the model surface and tunnel wall pressure data.

The system is capable of traversing all three probes at preprogrammed positions, acquiring all necessary data automatically, and reducing basic quantities such as mean values on the real-time bases. At each measurement position, each quantity was sampled over an approximate duration of 20 s so that good averages could be obtained. The instantaneous hot-wire outputs were sampled and digitized real-time only to reduce the averages. Concurrently, the bandpass filtered signals between 1 and 20 kHz were recorded on magnetic tape for an off-site digital analysis to obtain turbulence quantities. The off-site analysis of the hot-wire signals included digitizing

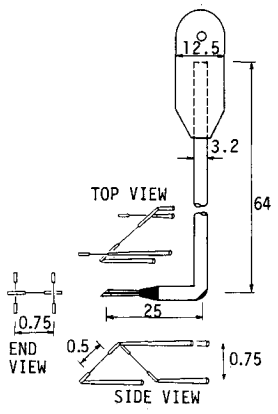

Fig. 2. Triple-wire probe, mm.

the signals at 40 kHz converting into instantaneous velocity and averaging using a system based on a PDP/11 minicomputer.

Test Flow Conditions

General Test Flow Conditions

After a brief survey of the lift characteristics of the present high-lift model, two test conditions with three-segment configurations have been selected for the detailed flowfield survey, as summarized here:

	Test Case A	*Test Case B*
Re	3×10^6	3×10^6
Ma_{ref}	0.2	0.2
α (angle of attack)	10 deg	18 deg
δ_s (slat deflection)	30 deg	30 deg
G_s (slat gap)	3.14%	3.14%
O_s (slat overhang)	−3.0%	−3.0%
δ_F (flap deflection)	15 deg	30 deg
G_F (flap gap)	2.27%	2.18%
O_F (flap overhang)	2%	1%
BLC	Off	On

Test case A is a condition that is close to a takeoff configuration with 15-deg flap deflection with a moderate C_L of 2.8. The boundary layers are all attached and the wake is expected to be of moderate thickness. Test case B is a much higher lift coefficient case with higher angle of attack and larger flap deflection. In both cases the freestream Mach number was kept constant at 0.2, the freestream temperature was held at about 90°F, and the tunnel pressure was adjusted to give a nominal chord Reynolds number of 3×10^6. The drag coefficient C_D obtained from the five-hole probe data at the most downstream wake stations was 0.033 and 0.069 for test cases A and B, respectively.

Two-Dimensionality of the Test Flow

The closeness of the flow to the two-dimensional condition was evaluated in a few different ways. Minitufts[11] were attached on the upper surface of the model and on the sidewalls to observe the direction and the movements of these tufts through a video camera. Generally, the indication of the minitufts in the present test conditions was that the flow directions on the surface did not vary in the spanwise direction, except near the model sidewall juncture region. However, the results were not conclusive in regions where the local flow speed or the skin friction was small.

Figures 3a and 3b show the spanwise pressure distributions along the trailing edges of the main element and the flap with and without the sidewall boundary-layer control for test cases A and B, respectively. The pressure along the trailing edge of the main element is seen to be quite uniform, while that along the flap trailing edge shows some variation. The result along the main element trailing edge with BLC on or off were almost the same, and only one set of results are shown. The pressure near the right-hand wall is very low, indicating a possible separation of the boundary layer on this wall. The magnitude of the spanwise nonuniformity, excluding these extreme values near the right sidewall, is seen to be less than 5% of the total C_p variation over the entire model. The sidewall boundary-layer control appears to be ineffective for test case A as far as reducing the spanwise variation of surface pressure. In test case B, however, the spanwise uniformity is improved when the blowing control is on. Furthermore, the turbulence data in the wake indicated that the sidewall blowing moved the wake position slightly and increased the turbulence intensity in test case A. Based on this observation, it was decided to leave off the BLC while the probe traverse data of test case A were taken and to turn on the BLC while the data of case B were obtained. An additional run with all brackets on showed that the mean velocity profiles are not influenced at all, but the Reynolds stresses are seen to be slightly higher.

Effects of Probe Traverser

There are a few separate ways in which the probe traverser influences the flow. The first is the overall blockage of the tunnel flow. When the primary traverser is in the vertical position, the projected area of the traverser structure in the tunnel flow direction is nearly 5% of the total tunnel cross section. Most of this effect, however, can be canceled out by nondimensionalizing with the appropriate "freestream velocity." The direct disturbance due to the probe and the stem is confined within narrow wakes of the probes and stems. The disturbances did not trigger large-scale changes of the flow structure, such as the shifting of boundary-layer transition and separation points.

The modification of the near-field pressure can be examined by comparing the surface pressure distributions for different traverser positions. The positions and orientations of the traverser are so distinct when surveying various parts of the flow that if the blockage due to the traverser is significant, its effect must show in the surface pressure distributions taken while surveying different parts of the flow. Figures 4a and 4b show the surface pressure distributions while the upper-surface boundary layer, the wake, and the lower-surface boundary layer are surveyed for the two test conditions. The order of magnitude of the differences among the results for different traverser positions is representative of the order of magnitude of the disturbances created by the probe traverser and is comparable to the spanwise nonuniformity of the trailing-edge pressure, as shown in Fig. 3.

Measurement Accuracy

Estimates of the accuracy of the presented data, measurement uncertainties based on calibration results, and preliminary measurements made by using the present instrumentation are given here. The mean velocity data, both five-hole probe and hot-wire data, are considered to have accuracies better than 2%, except in the following regions where the error can be larger but is expected to be smaller than 5% of the local value or the reference velocity, whichever is larger. They are the first station on the main element, inside

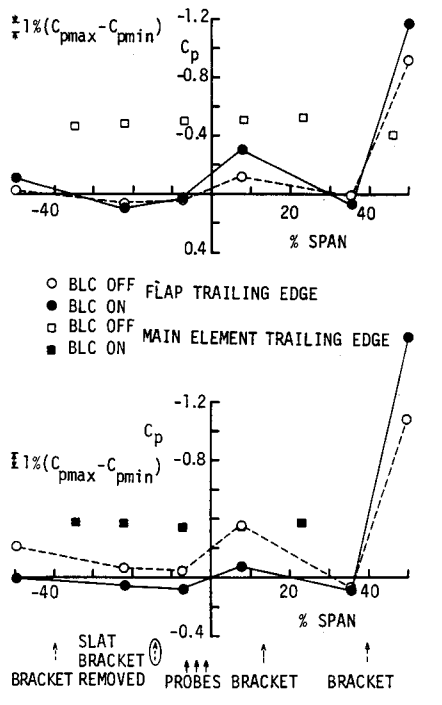

Fig. 3. Spanwise pressure distribution: a) test case A; b) test case B.

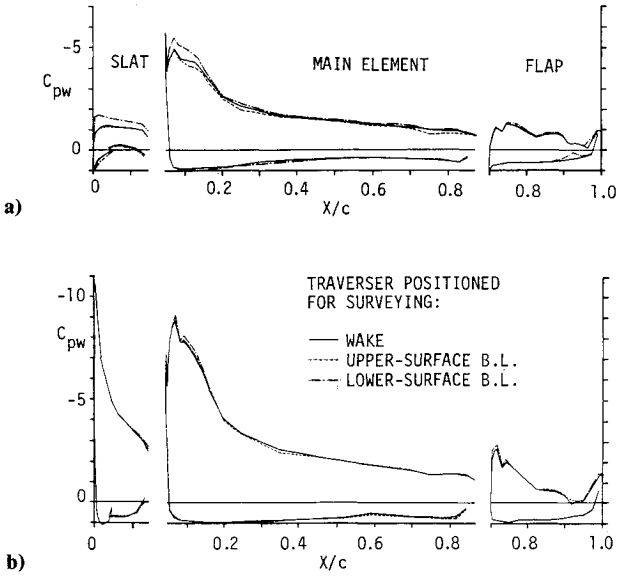

Fig. 4. Surface pressure distribution: a) test case A; b) test case B.

the flap well, near the flap nose, and in the flap trailing-edge regions. The flat-tube data are accurate to 2% within a few millimeters from the surface, and the data in most other areas, although acquired, have not been used for any purpose. The turbulent stress data are suspected to be accurate to only within 5% of the maximum within a profile in general and to about 10% in the trailing-edge high-turbulence regions.

Results

In the presentation of the results, the coordinate x is defined to be the direction normal (positive downstream) to the traverse direction, while y is the coordinate in the direction of traverse and z is the spanwise coordinate completing the right-hand coordinate system (x,y,z). The mean velocity components in the x, y, and z directions are denoted by U, V, and W, respectively. The fluctuating velocity components are designated by the corresponding lowercase letters. In the designation of a station, X means the chordwise distance from the leading edge of the slat that the point on the body would have if all segments were in the stowed position. The $X/c = 0.8$ station on the flap that is extended, therefore, is more aft of the $X/c = 0.8$ station on the main element. The expression $X/c = 1.0$ means the trailing edge of the flap. In the wake, $X/c > 1.0$ and is measured along the extension of the chord line on the flap. Expression $y = 0$ is taken along this line. The traverse directions are taken to be roughly perpendicular to the general local flow direction.

Mean Velocity Data

Figures 5a and 5b show overall views of the main velocity fields. These are the vector plots of the hot-wire mean velocity data. The overall flow features, including some details of velocity profiles and local flow directions, are well represented in these plots. Particularly, features of merging shear layers, flow curvatures in the near wake, and flow properties in the flap-well area should be noted. In each test case, the flows are seen to be attached to the model surfaces, except for the flap-well cavity area.

Some of the individual mean velocity profiles obtained by the five-hole and flattened pitot probes as well as the hot-wire data are shown in Figs. 6 and 7. The five-hole and triple-wire probes give all three velocity components U, V, and W, while the flattened probe gives only U. The overall agreement among different probe results is good. The boundary layer on the lower surface of the flap in test case B was too thin to be detected by any probe and no traverse was done there.

The logarithmic law of the wall could be identified in the data taken by the flat-tube probe in the upper surface boundary layer of the main element. The skin-friction coefficient C_f was determined whenever the log law was discernible by fitting it with the standard log law. The results are plotted in Fig. 8 to show the variation with chordwise distance. The same figure shows the variation of the "edge velocity" U_e used in the definition of C_f. The quantity U_e is the value of U at the outermost edge of the shear layers as measured by the five-hole probe. On the main element, C_f is never smaller than 0.0015 and the boundary layer is far from separation. In fact, near the trailing edge C_f is seen to recover slightly in both test cases.

Inflow Static Pressure

The static pressure within the shear layers of high-lift systems is known to vary considerably more than in flows around single airfoils. This static pressure variation is a necessary result of the high-lift condition with large-pressure difference between the upper and lower surfaces. It is also a result of thick shear layers due to confluent wakes of upstream elements and the boundary layer of a downstream element. It is important to know to what extent the static pressure varies and to examine the implication for computational methods. In the present investigation the static pressure in the flowfield has been obtained from the five-hole probe data, as explained earlier.

Figures 9a and 9b show the results for test cases A and B, respectively. The plotted pressure data within one streamwise station are the deviations from the local surface value in the case of surface-bounded stations and from the tunnel freestream static pressure in the case of wake stations. In both cases they are normalized by the tunnel dynamic pressure. It is clearly seen that the static pressure does vary significantly, say more than 10% of the dynamic pressure, across various parts of the shear layers. The generally positive pressure gradients above the model and negative gradients in the near wake are as expected. However, a few other features are seen in these figures. First, the normal pressure gradient due to the surface curvature near the leading edge of the main element where the slat wake is significant is very large. Second, a sharp, almost steplike change in static pressure can be seen in the region between the trailing edge of the main element and the flap leading edge. This rapid change of static pressure is due to the fact that the suction peak in the flap leading edge is much lower than the pressure at the main-element trailing edge. Finally, the total magnitude of static pressure variation in the near wake in test case B is seen to be as large as 40% of the tunnel dynamic pressure. There, normal pressure gradients are so large by conventional boundary-layer standard that no analysis method can ignore these effects.

Turbulent Stresses

Representative individual profiles of turbulent stresses are shown in Figs. 10 and 11. Figures 12a, 12b, and 12c present the composite profiles of $\overline{u^2}$, $\overline{v^2}$, and $\overline{uv}$ of test case A, respectively. It should be remembered that $\overline{uv}$ is the correlation between the fluctuating velocity components in the x and y directions, respectively. Here, y is generally the direction of the traverse, normal outward from airfoil surfaces and approximately perpendicular to the flow direction in the wake. The quantity $\overline{uv}$ is known to depend very much on the choice of coordinates,[9] and proper interpretation must be made. Although no direct verification of the results is possible in such complex flows, the results appear plausible, at least at positions where they can be estimated from simpler known flows. The qualitative shapes of the profiles in other areas are consistent with explainable mechanisms. The complex profiles with multiple local minima and maxima in the downstream region correspond, although very roughly, to the mean veloc-

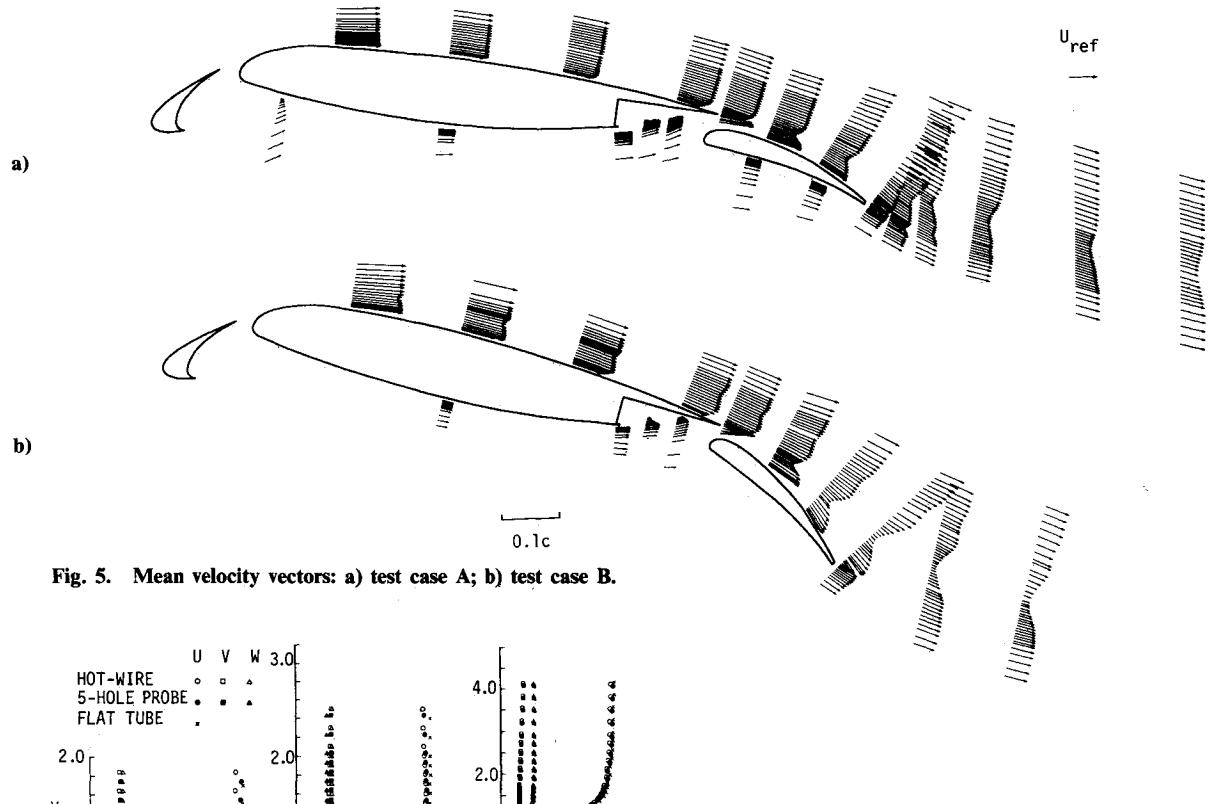

Fig. 5. Mean velocity vectors: a) test case A; b) test case B.

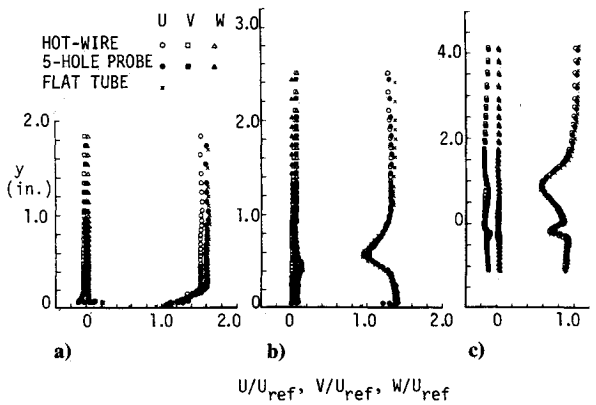

Fig. 6. Representative mean velocity profiles, test case A: a) main element upper surface, $X/c = 0.4$; b) flap upper surface, $X/c = 0.8$; c) wake, $X/c = 1.5$.

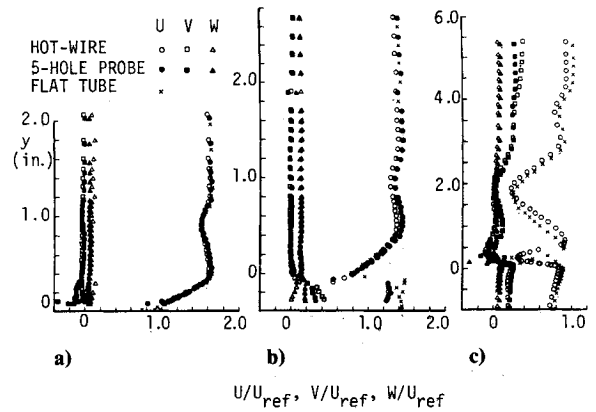

Fig. 7. Representative mean velocity profiles, test case B: a) main element upper surface, $X/c = 0.6$; b) main element trailing edge, $X/c = 0.88$; c) wake, $X/c = 1.01$.

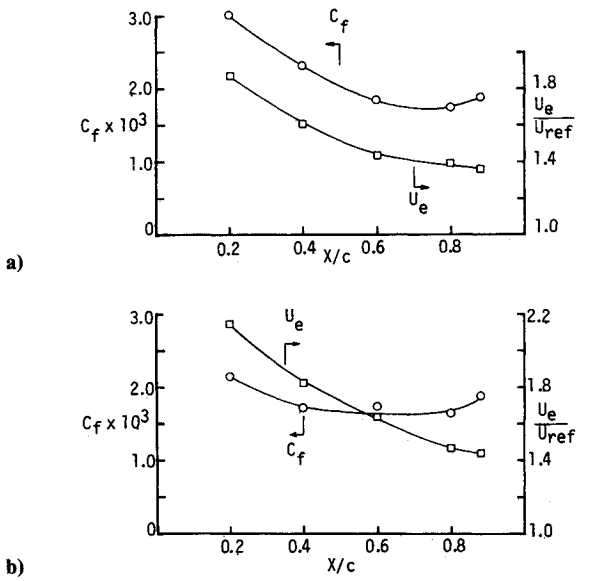

Fig. 8. Skin-friction coefficient and edge velocity distributions in upper surface boundary layer: a) test case A; b) test case B.

ity gradients. The ripples in the shear-stress profiles reflect the merging shear layers better than the mean velocity profiles.

The magnitudes of the stresses in the near wake in both test cases are seen to be very high. The spanwise fluctuation in test case B, in particular, is very high. It is interesting to note that the turbulence in the wake of the slat is smaller in test case B, although the wake strength, implied by the mean velocity data, is larger, perhaps due to the increased convex curvature effects that tend to suppress turbulence.

As for the relative magnitudes of the different components, the streamwise fluctuations $\overline{u^2}$ are the largest at most stations as expected, but there are stations where the spanwise fluctuations are larger. The transverse fluctuations $\overline{v^2}$ are seen to be the smallest in general.

Discussion

The flowfield is very complex, and discussion of the results will be given for individual regions of the flow after a brief description of the overall flowfield properties.

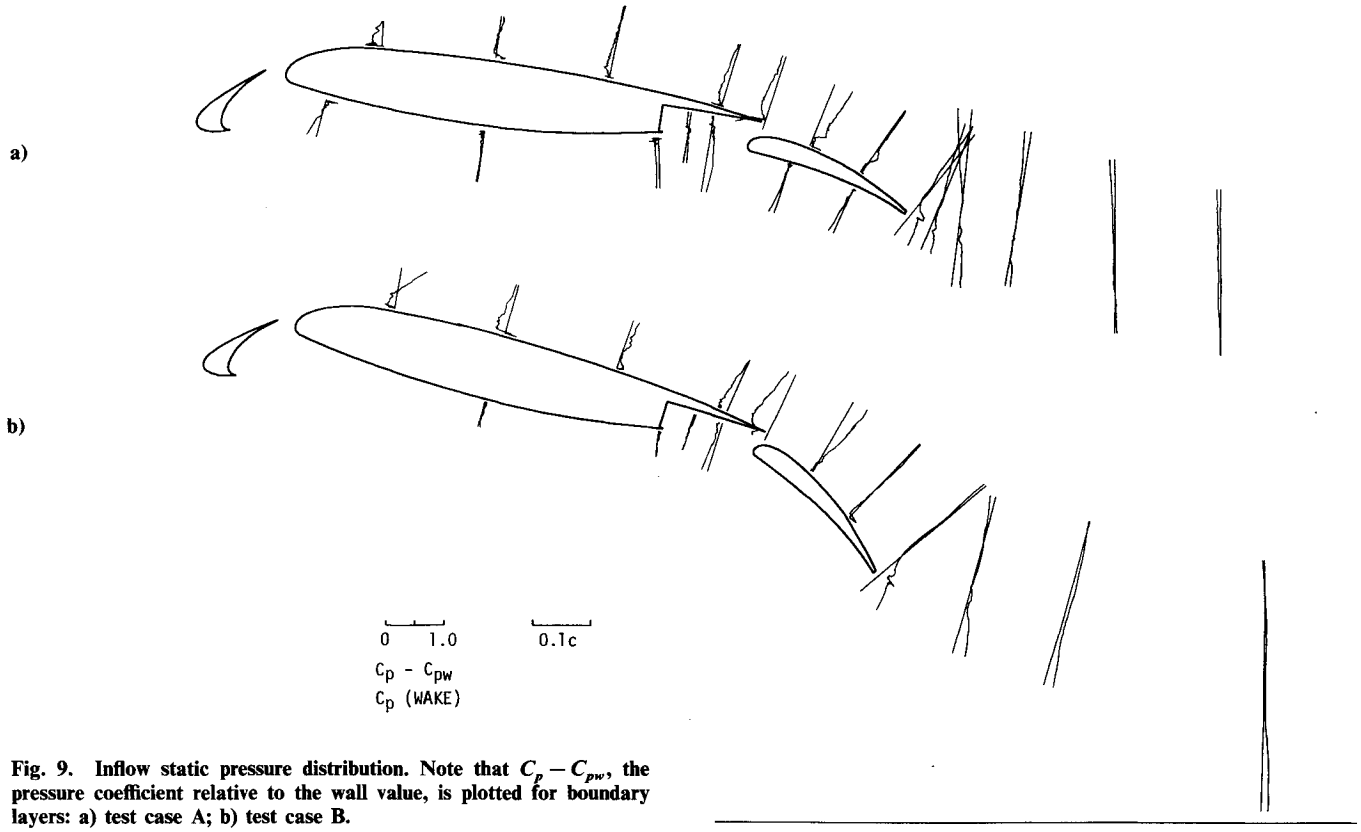

Fig. 9. Inflow static pressure distribution. Note that $C_p - C_{pw}$, the pressure coefficient relative to the wall value, is plotted for boundary layers: a) test case A; b) test case B.

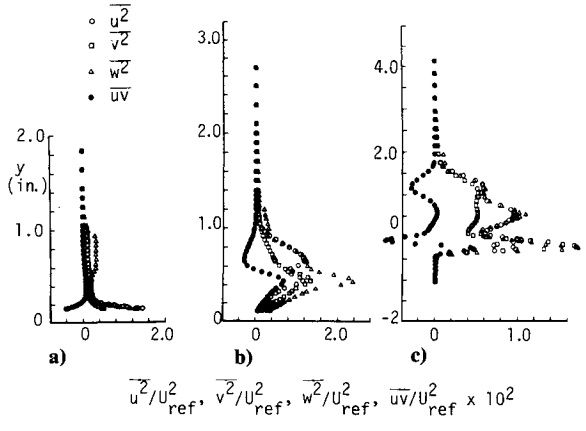

Fig. 10. Representative turbulent stress profiles, test case A: a) main element upper surface, $X/c = 0.4$; b) flap upper surface, $X/c = 0.8$; c) wake, $X/c = 1.05$.

Overall Flowfield

The overall flowfield is best visualized in the velocity vector plots of Figs. 5a and 5b. In both cases there is no flow separation, except for separation bubbles that necessarily exist inside the flap-well region and the underside of the slat. Generally, the shear flows on the lower surfaces are negligibly thin compared with those on the upper surface and in the wake, so emphasis is placed on discussion of flows above upper surfaces. Flow around the slat is not measured since it is either a very thin laminar boundary layer or a small separation bubble, either of which is difficult to measure using the present instrumentation. However, the present data at the most upstream measurement station can be used as initial conditions for testing the shear-flow computations. The shear flows are so unconventional that calculation and even definition of boundary-layer-type parameters was not only impossible but perhaps even meaningless in most locations. Boundary-layer-type analyses were done only on the flow over the upper surface of the main airfoil.

Slat Wake

The mean velocity vector plots indicate that the wake of the slat is very small and even difficult to identify in test case A while the slat wake in test case B is significant. The strength appears to be connected with the total load on the slat, which is considerably smaller in test case A. Its development in the downstream region is seen to be related to the pressure gradient along its path. The wake in test case A shows a monotonic decay as it passes the main element and the flap. In test case B, however, the wake grows in the region over the flap where there exists a significant adverse pressure gradient.

The initial development of the slat wake is influenced strongly by the acceleration and curvature due to the leading edge of the main foil. The inflow static pressure variations shown in Figs. 9 indicate that even the cross-stream pressure variation is very large. The effects of the curvature and the pressure gradients are seen more clearly in the turbulence data. The near-symmetric distribution of the normal stresses and antisymmetric shear-stress distribution about the wake center of test case A and highly asymmetric stress distributions in test case B, respectively, are considered to be caused by the curvature effects. In the leading-edge region of the main foil, the upper half of the wake is stable and the lower half is unstable based on the stability criteria of curved flows. In test case B, in which this turning is much more intense, the stable half of the wake is seen to have collapsed completely, while the turbulence on the unstable side is very large. Prediction of this type of skewed wake will be very difficult.

Boundary Layer on Main Airfoil

The main difference between the boundary layer on the main airfoil and boundary layers on single airfoils is that in the former case, there is a wake of the upstream slat that influences boundary-layer development. The velocity profiles indicate that the shear-layer interaction is weak. It appears that under realistic conditions such as the present ones, the

streamwise distance over the main airfoil is not long enough for a significant merging or intense interaction to take place, or else as in the present test case A, the wake of the slat diminishes before any significant merging occurs. This is a rather favorable feature for computation of such flows, since superposition of defect velocities in isolated flows may be used as reasonable approximations.[12-15] On the other hand, the turbulence data shown in Fig. 12 indicate that the turbulence in the slat wake is not negligible and does have influence on the boundary-layer development.

Quantity C_f, shown in Fig. 8, indicates that unlike the situation on the upper surface near the trailing edge of single airfoils where C_f usually continues to drop, C_f rises near the trailing edge. This C_f recovery occurs even with continued decrease in U_e, and part of the reason may be the indirect effect of the merging.

Flow around the Flap

The flow around the flap is very complex, as can be seen from the mean flow data. This flow may be interpreted as the interaction and merging of at least three layers with vastly different natures. The outermost layer is the wake of the main airfoil combined with the wake of the slat. The middle layer is the jetlike accelerated flow issuing through the gap. The nature of this part of the flow, however, is very different from that of wall jets, which are usually driven by pressure and are often well-developed turbulent flows. The flow through the gap is a highly accelerated potential flow, and the pressure here is low compared with the outer layer, which creates an enormous normal-to-flow pressure gradient. The innermost layer is the boundary layer developing on the flap. Due to the strong favorable pressure gradient and convex curvature, this boundary layer tends to stay thin and laminar.

Near the trailing edge of the flap, all these layers interact with each other, resulting in a very complex shear flow. The largest contributor is the wake of the main element in terms of the mean velocity profile and turbulent stress. Although the present gap and overhang are not optimum, they are not far from it and imply that the potential flow at the slot exit exists and persists over about half of the flap chord, for near-optimum gap settings.

Wake

The present measurements include the details of the complex near wake and the intermediate wake, where most of the smoothing in the velocity profiles and most of the turning take place. The wake at the most downstream position, however, may not be called the "far wake," where characteristics can be represented by a single parameter.

The distinct characteristics of the wake of multielement airfoils, as opposed to single airfoils, are that the near wake is very thick due to the confluent multiple wakes and the wake curvature is large. The details of these features are well exhibited in the presently obtained data of the two test cases. The mean velocity data show that just downstream of the trailing edge, the wakes of different elements have started

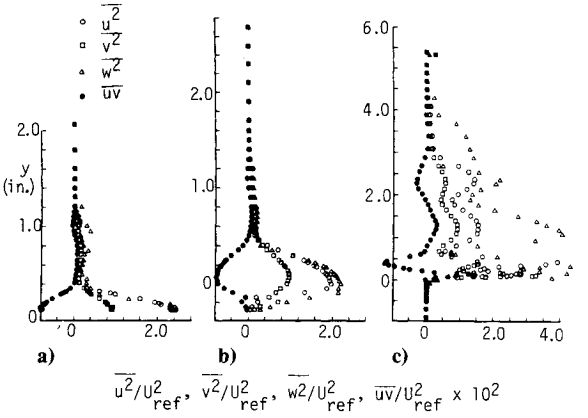

Fig. 11. Representative turbulent stress profiles, test case B: a) main element upper surface, $X/c = 0.6$; b) main element trailing edge, $X/c = 0.88$; c) wake, $X/c = 1.01$.

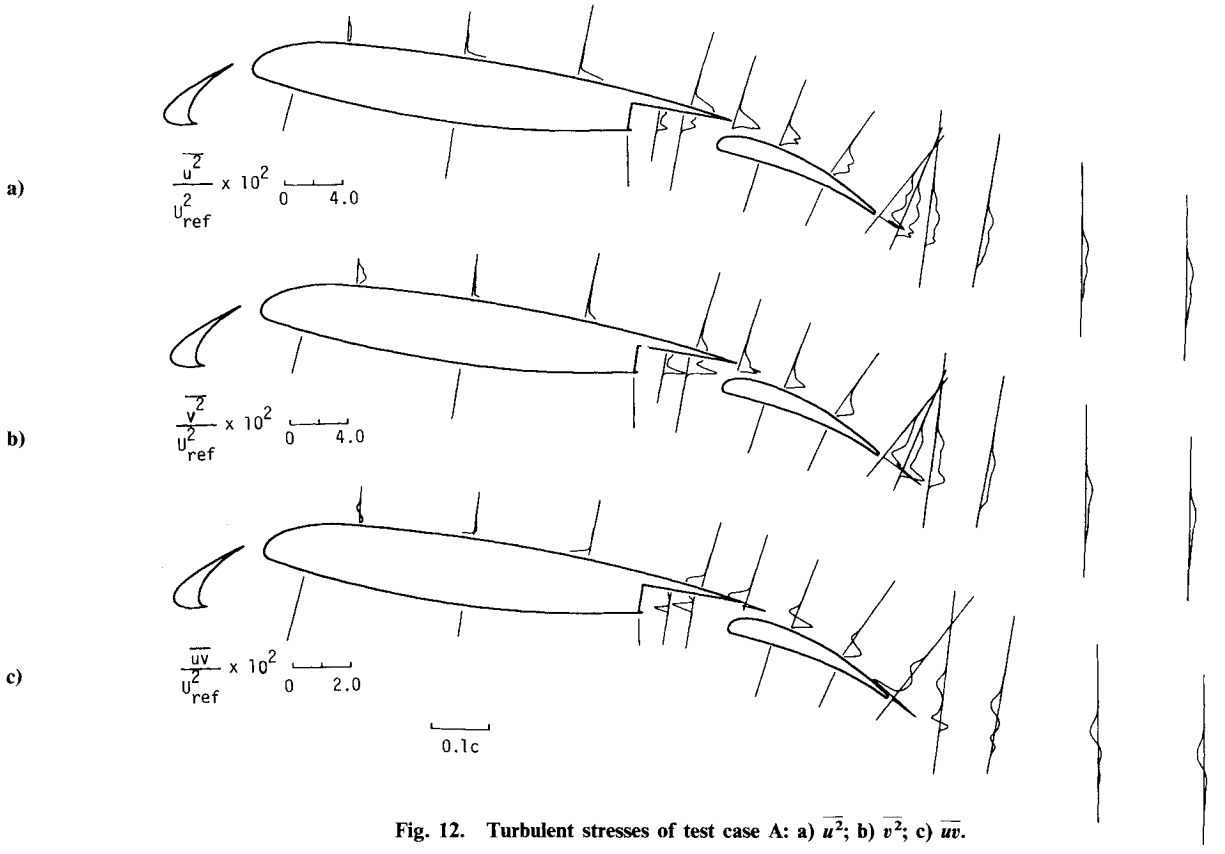

Fig. 12. Turbulent stresses of test case A: a) $\overline{u^2}$; b) $\overline{v^2}$; c) $\overline{uv}$.

merging, but the merging is only partial and individual component wakes can still be identified. In each test case the wake of the main element is the strongest one, and the other two wakes appear to be absorbed by this main wake as the wake develops. This means that the overall wake path may be much different from a smooth extension or theoretical "inviscid-flow" streamline leaving the trailing edge of the most downstream element. It is seen clearly in the data of test case B that the "wake center" is located at much higher positions than the extension of the flap trailing edge. The wake of the flap, however, is seen to diminish quite rapidly in both cases. The effects of the streamline curvature on the lower side of the wake are such that the turbulence is attenuated, and may be contributing to this rapid disappearance of the flap wake. The turbulent shear-stress data do show these curvature effects.

The data of Braden et al.[3] indicate that the initial flow separation occurred in the wake of the main element, which suppressed the flap loads. It has also been pointed out by Johnston and Horton[15] that the stall of a high-lift system may not occur as a separation of the boundary layer on the flap (as found by Adair and Horne[4] on a simple-shaped but not very efficient flap), but as the recirculation in the wake penetrates into the flow above the flap. Smith,[16] based on a crude analysis, speculated this possibility but expected that in practice, the boundary layer on the surface is more susceptible to separation than the wake. The present data of test case B suggest that this may not be the case. Test case B is far from stall, but it is seen that the velocity in the central part of the near wake is decreased to as low as about 20% of the external value, while there is no indication of flow reversal on the flap surface. This central portion of the near wake may be considered very close to local flow reversal. In fact, if we take into consideration that rather large turbulent fluctuation is superimposed on this mean value and that either of the presently used probes does not respond to temporarily reversing flow, the actual mean velocity may be even smaller than measured. It can be anticipated that with slightly more deflection of the flap the local flow may actually reverse.

The flow reversal in the wake may be explained by the effects of the strong adverse pressure gradient in the environment of small shear stresses. This feature, which has not been stressed, will have an impact on methods of computing these flows with a detached recirculation region.

Conclusions

Detailed measurements of mean flow and turbulence quantities have been made using pressure and hot-wire probes in the shear flow regions around high-lift multielement airfoil in two test conditions in order to study the characteristics of the complex turbulent shear flows. The model configuration in both test cases was a three-element one with a slat and a flap.

The data reveal a number of features of shear flows around high-lift systems. Although there is no major separation even at high angle of attack, the shear flow regions above the flap and in the near wake are very thick and considerable static pressure variation exists. There are several regions where curvature effects are strong.

Generally, the wake of the main airfoil is the strongest and the wakes of other elements are absorbed in it, thus widening the entire wake width. The wake center, therefore, is along a highly curved trajectory starting at the trailing edge of the main element and not at the trailing edge of the most downstream element. There is an indication that flow reversal will first appear in the wake rather than in the boundary layer on the flap. The wake of the slat or, more correctly, the turbulence in the slat wake appears to have an important effect on the development of the boundary layers on the main element, in particular on transition from laminar to turbulent flow.

Overall, the data indicate that the shear flows are so different from classical shear layers that very general methods, both equations and the turbulence model, will be required. The present results suggest strongly that further work is necessary to obtain similar data with better two dimensionality of the overall flow at higher Reynolds number and at higher C_L conditions, including landing configuration. It also suggests a number of more basic studies that should be performed to improve understanding of specific flow mechanisms.

Acknowledgment

This work was done as part of a cooperative program between Douglas Aircraft Company and NASA Langley Research Center.

References

[1]Cebeci, T., Stewartson, K., and Whitelaw, J. H., "Calculation of Two-Dimensional Flow Past Airfoils," *Numerical and Physical Aspects of Aerodynamic Flows II*, edited by T. Cebeci, Springer-Verlag, New York, 1984.

[2]Olson, L. E. and Orloff, K. L., "On the Structure of Turbulent Wakes and Merging Shear Layers of Multielement Airfoils," AIAA Paper 81-1248, June 1981.

[3]Braden, J. A., Whipley, R. R., Jones, G. S., and Lilley, D. E., "Experimental Study of the Separating Confluent Boundary Layer," NASA CR-3655, 1983; also AIAA Paper 86-0505, Jan. 1986.

[4]Adair, D. and Horne, W. C., "Turbulent Separated Flow in the Vicinity of a Single-Slotted Airfoil Flat," AIAA Paper 88-0613, Jan. 1988.

[5]Seetharam, H. C. and Wentz, W. H. J., "A Low-Speed Two-Dimensional Study of Flow Separation on the GA(W)-1 Airfoil with 30-Percent Chord Fowler Flap," NASA CR-2844, May 1977.

[6]Van den Berg, B., "Boundary-Layer Measurements on a Two-Dimensional Wing with Flap," Rept. NLR TR79009U, National Aerospace Laboratory, Amsterdam, Jan. 1979.

[7]McGhee, R. J., Beasley, W. D., and Foster, J. M., "Recent Modifications and Calibrations of the Langley Low-Speed Pressure Tunnel," NASA TP-2328, July 1984.

[8]Stainback, P. C. and Owen, F. K., "Dynamic Flow Quality Measurements in the Langley Low Turbulence Pressure Tunnel," AIAA Paper 84-0621, Jan. 1984.

[9]Nakayama, A., "Flowfield Survey Around High-Lift Airfoil Model LB546," McDonnell Rept. MDCJ4827, Feb. 1987.

[10]Treaster, A. L. and Yocum, A. M., "The Calibration and Application of Five-Hole Probes," *ISA Transactions*, Vol. 18, No. 3, 1979, pp. 23–34.

[11]Crowder, J. P., "Fluorescent Minitufts for Nonintrusive Flow Visualization," McDonnell Douglas Rept. MDC J7374, Feb. 1977.

[12]Pot, P. J., "A Wake Boundary Layer Mixing Experiment," *Proceedings of the 2nd Symposium on Turbulent Shear Flows*, Imperial College, London, 1979.

[13]Zhou, M. D. and Squire, L. C., "The Interaction of a Wake with a Turbulent Boundary Layer," *Aeronautics Journal*, Vol. 89, Feb. 1985, pp. 72–81.

[14]Nakayama, A., Akdag, V., Liu, B., and Unt, H., "Wake-Boundary Layer Merging Experiment," *AIAA Journal* (submitted for publication), 1987.

[15]Johnston, L. J. and Horton, H. P., "An Experimental Study of Turbulent Wake/Boundary-Layer Mixing Flows," *Proceedings of the International Council of the Aeronautical Sciences*, 1986, pp. 360–369.

[16]Smith, A. M. O., "High-Lift Aerodynamics," AIAA Paper 74-939, Aug. 1974.